PAPER

Check for updates

Average collision velocity of single yeast cells during electrochemically induced impacts†

John A. Lutkenhaus,[a] Junaid U. Ahmed,[b] Mehedi Hasan,[a] Derek C. Prosser[c] and Julio C. Alvarez [ID] *[a]

We recorded current–time (i–t) profiles for oxidizing ferrocyanide (FCN) while spherical yeast cells of radius ($r_c \approx 2$ μm) collided with disk ultramicroelectrodes (UMEs) of increasing radius ($r_e \approx 12$–45 μm). Collision signals appear as minority steps and majority blips of decreased current overlayed on the i–t baseline when cells block ferrocyanide flux (J_{FCN}). We assigned steps to adsorption events and blips to bouncing collisions or contactless passages. Yeast cells exhibit impact signals of long duration ($\Delta t \approx$ 15–40 s) likely due to sedimentation. We assume cells travel a threshold distance (T) to generate collision signals of duration Δt. Thus, T represents a distance from the UME surface, at which cell perturbations on J_{FCN} blend in with the UME noise level. To determine T, we simulated the UME current, while placing the cell at increasing distal points from the UME surface until matching the bare UME current. T-Values at 90°, 45°, and 0° from the UME edge and normal to the center were determined to map out T-regions in different experimental conditions. We estimated average collision velocities using the formula $T/\Delta t$, and mimicked cells entering and leaving T-regions at the same angle. Despite such oversimplification, our analysis yields average velocities compatible with rigorous transport models and matches experimental current steps and blips. We propose that single-cells encode collision dynamics into i–t signals only when cells move inside the sensitive T-region, because outside, perturbations of J_{FCN} fall within the noise level set by J_{FCN} and r_c/r_e (experimentally established). If true, this notion will enable selecting conditions to maximize sensitivity in stochastic blocking electrochemistry. We also exploited the long Δt recorded here for yeast cells, which was undetectable for the fast microbeads used in early pioneering work. Because Δt depends on transport, it provides another analytical parameter besides current for characterizing slow-moving cells like yeast.

[a]Chemistry Department, Virginia Commonwealth University, Richmond, VA, 23294, USA. E-mail: jcalvarez2@vcu.edu
[b]Chemistry Department, Khulna University of Engineering and Technology, Bangladesh
[c]Biology Department, Virginia Commonwealth University, Richmond, VA, 23294, USA
†Electronic supplementary information (ESI) available: *i*–*t* curves for cells, voltammetry of mediator, COMSOL simulation report, microscope images, cell-size distribution. See DOI: https://doi.org/10.1039/d4an00134f

Introduction

Stochastic blocking electrochemistry is a method whereby colliding nano- and microparticles block the electrochemical reaction of an electroactive mediator reacting at an ultramicroelectrode (UME).[1–3] Of the methods relying on single particle impacts,[4] stochastic blocking electrochemistry represents the most universal[5] because it detects collisions of insulating[1,2] and conductive particles.[6] Typically, the collision signal appears overlayed on the current–time (i–t) baseline recorded for mediator response.[1–3] For example, an adsorptive

impact gives rise to a "sudden" decrease (step) in current (Δi) on the i–t baseline, denoting a discrete disruption of mediator flux to the UME.[1–3] Since the first report in 2004,[1] research efforts have primarily focused on unveiling quantitative relationships connecting Δi with particle size,[2,3] or dependence of collision frequency (f) on particle transport and concentration.[5,7–10] However, very little attention has been paid to extracting information from the shape and duration (Δt) of signals during collision events.[11,12]

Here, we combine experiments and simulations to reveal how sensitivity arises in stochastic blocking electrochemistry and extract average collision velocities using a non-transport model. We exploit the long collision duration ($\Delta t \approx$ 15–40 s) recorded here for yeast cells, which was undetectable for the fast microbeads used in early pioneering studies.[1–3] The work described below closely relates to our recent report on rod-shaped bacteria (bacilli), wherein single adsorptive impacts exhibited duration intervals ($\Delta t \approx$ 0.6–1.1 s) scaling up with bacillus length.[12] We regarded Δt as the time spent arriving to the UME edge from a threshold distance (T), at which pertur-

bation of mediator flux begins contributing to the current step Δi.[12] To determine T, we simulated the UME current, while placing the bacillus at increasing distal points normal to the UME edge until matching the bare UME current.[2,3] Average velocities of cell arrival at 90° to the UME edge were calculated using the expression $T/\Delta t$.[12] Our calculated average values were congruent with rigorous transport models,[5,7] whereby a large bacillus particle electromigrates faster than a small one, due to decreased influence of diffusional fluctuations.[5,7]

In this work, we focus on spherical yeast cells of radius (r_c) ~2 μm. We recorded i–t profiles for oxidizing ferrocyanide (FCN) while the cells collided with Pt-disk UMEs of increasing radius (r_e = 6, 12.5, 15, and 22.5 μm). The positive potential applied to the UME for oxidizing FCN and the negative charge (zeta potential = −16 ± 4 mV) of the cells, drive them to electromigrate towards the UME edge,[3,13–15] against slight sedimentation.[16] The new important findings from this work can be summarized as follows: (a) T-values determined at 90°, 45°, and 0° on the UME edge (Scheme 1) allow us to estimate constant velocities using the formula $T/\Delta t$ and simulate arrival and retreat trajectories to match current steps (adsorption events) and current blips (bouncing collisions and contactless passages). (b) When the simulated ratio, r_c/r_e approaches ~0.7, the difference in Δi at the center and edge of the UME ("edge effect"), is predicted to vanish.[10] (c) Finally, we hypothesize that yeast cells encode their collision dynamics into current amplitude (Δi), duration (Δt), and signal shape, only when cells perturb the flux of ferrocyanide (J_{FCN}) inside a T-bounded region. Therefore, outside this region, cell motion becomes undetectable because flux perturbations fall within the noise level set by J_{FCN} and r_c/r_e, (Scheme 1). T-regions can extend 1–3 cell diameters around the UME when increasing J_{FCN} and r_c/r_e.
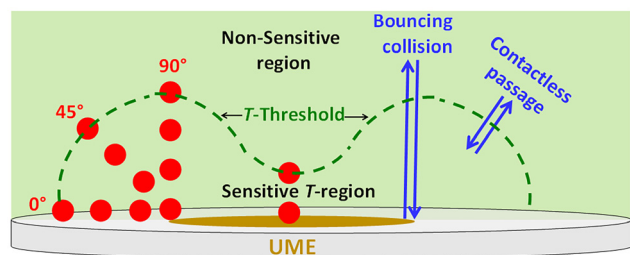
These results go beyond previous work,[2,3] because though simulations of T were made before,[2,3] we took the extra step of dividing T over the experimentally detected Δt to estimate average collisions velocities.[12] Not only do the values match the magnitude expected for particle electromigration in rigorous transport models,[7–9] but also the relationship of velocity and particle size agrees with the theory.[5,7,12] On the other hand, the trajectories simulated here are not expected to mimic experimental ones, because our velocities are averages, and actual particle velocities are non-constant due to the non-homogeneous electric field on the UME.[2,9] We believe this issue does not impair our analysis other than not knowing the actual trajectories, which would have to be confirmed by *in situ* correlated microscopy.[13,17]

Previous efforts to extract information from current step transients employed digital simulations of the sudden current drops from single adsorption events of polystyrene and platelet particles.[11] Likewise, UME-encircling regions of mediator flux (J_M) sensitive to "hovering" particles have been verified using optical tweezers.[18] For example, laser-trapped latex microbeads were slowly "levitated" and then "deposited" on UMEs under steady-state electrolysis.[18] The researchers demonstrated that the steady-state current (i_{ss}) changes its value when particles hinder J_M not just in contact with the UME, but also during contactless passages at distances lower than the UME radius.[18] Here, we systematically map out this J_{FCN}-sensitive region for various experimental conditions by determining T, normal to the UME center, and at three angles on the UME edge (Scheme 1). Though we have not worked out a mathematical relationship connecting J_{FCN} (or current, r_c/r_e) to T, the latter constitutes a useful qualitative concept to understand how cells encode collision signals and engender sensitivity in stochastic blocking electrochemistry.

This work represents a step forward in the quest to extract quantitative information from collision signals as well as uncovering factors that control sensitivity and accuracy in stochastic blocking electrochemistry.[5,7] We estimated average velocities at one of three trajectories (angles) towards the UME edge (Scheme 1). The angle was chosen applying sum of least squares analysis. We used the linear velocity $T/\Delta t$ when match experimental current–time values in a collision signal to simulated current–distance points. For simplicity, we assumed cells "entered" and "left" the T-region along the same direction. In adsorptive events and bouncing collisions, the cell reached the surface, but not for contactless passages (Scheme 1). We emphasize that cell experimental velocities are different from our average values despite matching experimental traces. However, our goal was to demonstrate that our non-transport model renders velocity values and parameter relationships congruent with accepted transport models.[5,7] We performed these simulations to support the main hypothesis of the paper (result c, above) and use the long duration signals detected here that were not available for the systems studied in early pioneering work.[1–3]

We have been inspired by the original reports developing this technique[1–3] and all the efforts that came later to explain particle transport[5,7] and address the "edge effect problem". Those include using electrodes with hemispherical[19] and ring shapes,[14] plus coupling of solution reactions to the redox mediator.[20] We also drew upon the work on electrochemical blocking of bacteria,[8,12,13,16,21,22] and blood cells.[23]

Scheme 1 Sensitivity model for electrochemical blocking: dashed line encloses a sensitive T-region rendered by simulating UME currents with the cell (red circles) placed at increasing distal points until reaching the value of bare UME current along three directions on the UME edge and normal to the center. Cell motion outside this region becomes undetectable. Arrows indicate the type of collision besides adsorption (not shown) simulated to match experimental traces. T-regions can extend 1–3 cell diameters and grow in proportion to J_{FCN} and r_c/r_e.

Experimental section

Reagents

All chemicals were reagent grade and used without further purification. Millipore water (18.2 MΩ cm) was used for all electrochemical experiments. Potassium hexacyanoferrate(II), $K_4Fe(CN)_6$, potassium hexacyanoferrate(III), $K_3Fe(CN)_6$, ferrocenemethanol, and potassium chloride (KCl) were purchased from Sigma-Aldrich (St Louis, MO, USA). Platinum (Pt) wire was purchased from Advent Research Materials (Eynsham, England).

Cell culture

Yeast strain DPY2532 (*MATa his3Δ1 leu2Δ0 met15Δ0 ura3Δ0 swe1::KANMX6*) was inoculated into 5–10 mL of sterile yeast extract-peptone-dextrose (YPD) medium [1% (w/v) yeast extract, 2% (w/v) peptone, 0.01% (w/v) ʟ-tryptophan, 2% (w/v) ᴅ-glucose] and grown for approximately 24 hours in a 30 °C orbital shaking incubator at 250 rpm to reach late-logarithmic or stationary phase with optical density at 600 nm (OD600) of 1.60 ± 0.05.

Cell preparation

Cells were harvested after centrifugation at 3000 rpm for 3 minutes. The supernatant was removed and the cells were washed twice with the chosen experimental solutions of 100 mM KCl and desired concentration of $Fe(CN)_6^{4-}$ (ferrocyanide) or $Fe(CN)_6^{3-}$ (ferricyanide) before being resuspended. Cell counting and concentration were determined using a hemocytometer *via* optical microscopy. Fig. S1A (ESI†) portrays a microscope image of yeast cells (~4 μm diameter), some of which have buds that increasing their apparent diameter (~8 μm). Budding reflects the stage of the cycle in which the cells are harvested. The bimodal size distribution evaluated with the hemocytometer is shown in Fig. S1B (ESI†) for each mM-concentration of ferrocyanide (200, 300, and 400, plus 100 mM of KCl). Despite the electrolyte concentration, cells maintained their integrity.

Ultramicroelectrode fabrication

The disk-Pt UMEs were prepared according to previous literature.[24] Briefly, a glass capillary was dried at 120 °C for 2 hours. 1 cm long Pt-wire was cut and connected to copper wire using conductive epo-tek H_2OE parts A and B silver epoxy. Pt-wire diameters of 10 μm, 25 μm, 35 μm, and 50 μm were used. After drying at 100 °C for 12 hours, the wire was inserted in the capillary and dipped into a solution of 15% (w/w) *m*-phenylenediamine and Epon Resin 820. Further drying at 100 °C for 12 hours, sealed the opposite end of the capillary with Torr Seal epoxy parts A and B with a 2 : 1 ratio. The completed UME was gently polished on 600 grit sandpaper and then mirror polished with 0.05 μm alumina using DI water on micro-cloth pads. A steady-state voltammogram for 1 mM ferrocenemethanol and 100 mM KCl was recorded to determine the diameters of each fabricated UME. The diffusion coefficient used for ferrocenemethanol was 7.8×10^{-6} cm² s⁻¹.[24]

The diameters were calculated to be 12 μm, 25 μm, 30 μm, and 45 μm respectively. Variation in diameter from the original wire is attributed to imperfections when sealing. Fig. S2A (ESI†) shows a microphotography of the 25 μm-UME, while Fig. S2B† displays the cyclic voltammograms (CVs) obtained with that electrode at 200, 300, and 400 mM of ferrocyanide in 100 mM of KCl. The CVs recorded as a function of electrode radius are shown in Fig. S2C (ESI†), whose steady-state currents, produced diffusion coefficients of ferrocyanide near 7×10^{-6} cm² s⁻¹, similar to literature values.[25,26]

Instrumentation

All electrochemical experiments were recorded using a 660c potentiostat purchased from CH Instruments (Austin, TX, USA) in a three-electrode system. A 0.5 mm Pt wire and Ag/AgCl were used as counter and reference electrodes, respectively. Chronoamperometric (i–t) curves were recorded for 1000 s at +0.6 V *vs.* Ag/AgCl using 50 ms sampling interval and performed at least 5 times. ζ-Potential for cells was recorded using the Zetasizer Nano ZS purchased from Malvern Panalytical (Westborough, MA, USA). Micrographs were taken using a 40×–2500× Infinity Plan Compound Microscope with 8 megapixel USB digital camera from Amscope (Irvine, CA, USA).

Simulations

3D-digital modeling was done using the Electroanalysis Interface from COMSOL Multiphysics version 5.6.[12] The hemispherical space around the UME-solution including part of the shroud, was divided in half to perform the simulation on one side of the hemisphere and save computation time (Fig. S3, ESI†).[12] Two domains with different mesh size were set up around the UME, so that the inner one had a finer grid than the outer one.[12] The oxidation of ferrocyanide was simulated solving only the diffusional part of the Nernst–Planck equation.[12] To evaluate the simulation, we used the criterion of convergence, whereby the number of grid elements was increased until trials of the same simulation did not vary more than 2.1% (see ESI†).[12] This variation was also smaller than the experimental noise for a particular electrode size.

Results and discussion

Experimental response

Fig. 1 shows the i–t plots recorded for yeast while varying cell concentration (C_c), electrode radius (r_e), and concentration of ferrocyanide (C_{FCN}). The i–t recordings lasting 1000 s were run with 100 mM of KCl as supporting electrolyte and setting the UME potential at +0.6 V *vs.* Ag/AgCl to induce a steady state current (*i.e.* limited by mass transport) in the FCN-oxidation. This was corroborated with the CVs presented in Fig. S2B and C (ESI†). Per convention, we display negative currents upwards, thus, despite blips and steps appearing upwards, they represent drops in current. We attribute the dearth and low frequency of events to sedimentation induced by the
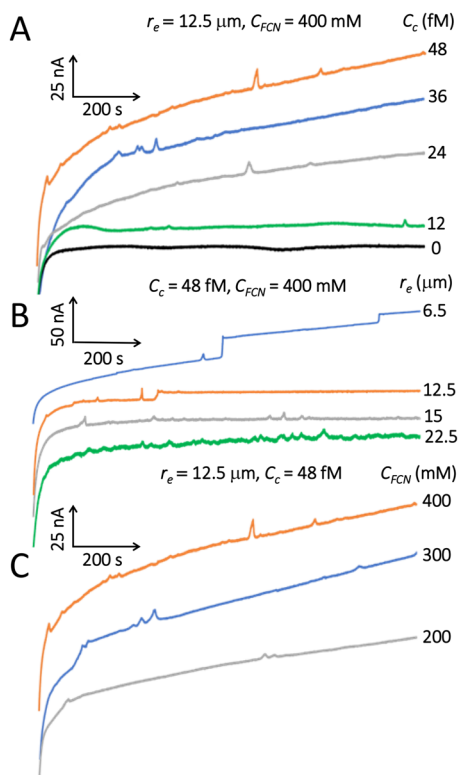
Fig. 1 $i–t$ response for yeast cells as a function of (A) cell concentration (C_c), (B) Pt UME radius (r_e), and (C) FCN concentration (C_{FCN}). Current blips and steps are drops in current despite being depicted upward. Solutions were 100 mM KCl and set to +0.6 V $vs.$ Ag/AgCl.

density of the cells,[16] as well as weakened cell electromigration. The latter results from the relative low zeta potential ($\sim$−16 mV) of the cells determined in our experiments, which is lower than what we measured for bacteria under equal electrolyte conditions (−42 to −56 mV).[12]
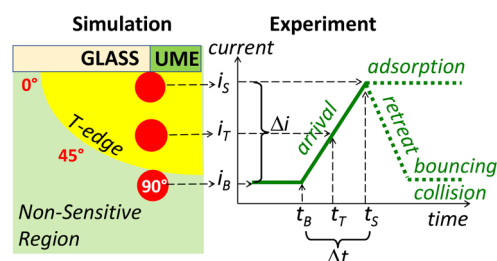
The effect of gravity was demonstrated in recent blocking electrochemistry experiments of yeast cells using 100 mM ferrocyanide and 0.85% NaCl electrolyzed with a 25 μm-diameter Pt UME.[16] The researchers placed the UME surface facing upwards at the bottom of a flipped electrochemical cell. When comparing the same yeast concentration, the "flipped" $i–t$ profile showed a drastic increase in collisions, all appearing as current steps, which makes us suggest that the minority steps and long transient blips observed in our experiments are the result of gravity acting on the cells.[16] The responses in Fig. 1 are very similar to the ones obtained in those studies.[16] Every trace in Fig. 1 was recorded five times, but the scarcity of events per trace precludes a reliable frequency analysis. Nevertheless, the plots reveal expected trends. For example, in Fig. 1A (r_e = 12.5 μm) the number of events increases as cell concentration grows starting with a blank sample free of cells. In Fig. 1B, cells collide more frequently on larger electrodes, albeit with noisier and lower amplitude (Δi) signals, even though the cell concentration was at the high limit (48 fM) to prevent cell aggregation. As observed with other blocking

particles,[1–3] the magnitude of the collision response (in this case blips) becomes more intense when increasing FCN concentration (Fig. 1C) because J_{FCN} surges as a result of a greater concentration gradient at the UME surface (see below). We assign the current blips to bouncing collisions and/or contactless passages because they have been observed using *in situ* microscopy for blocking impacts of bacteria.[8,13] The current steps are ascribed to adsorptive collisions as done previously.[8,12,13,21–23]

3D-digital simulations

Our goal here is twofold. First, we want to demonstrate that the non-transport model proposed here produces cell velocity values ($T/\Delta t$) and parameter relationships compatible with rigorous transport theory.[7] Second, we want to match current points in experimental impact signals (Fig. 1) using three collision types: adsorption, bouncing collision, and contactless passage. For simplicity, in the latter two, we mimicked cell "entry" and "exit" of the T-region in the same direction (Scheme 1).

Determination of T. We performed a 3-D finite-element modelling (see Experimental section and ESI†) following our approach for adsorptive impacts of bacteria,[12] which in turn was derived from pioneering simulations done with microbeads.[2,3] We first simulated the steady state current for bare UME ($i_{ss} = i_B$) oxidizing FCN in a potential step at +0.6 V for specified conditions of r_e and C_{FCN}.[12] Next, we simulated the cell as a sphere of radius 2 μm (or 4 μm) placed at the UME surface to generate the "*current with cell on the surface*" i_S (Scheme 2). Subsequently, we simulated currents while placing the cell at increasing distal points from the UME surface until the simulated current matched the value of i_B. The distance at which the current with cell matched the current without cell (i_B) was regarded as T. This is the demarcation edge of the T-region in yellow (Scheme 2). We performed this procedure at the UME edge in three directions, 90°, 45°, and 0° and normal to UME center. Any current simulated inside the T-region when the cell is not at the surface appears labelled as i_T in Scheme 2.

Scheme 2 (Left) Current (i) simulations with cell (red) as a function of distance: at surface (i_S), in T-region (i_T), and when matching the bare UME current (i_B) to determine T along three angles, 90°, 45°, and 0° (edge of yellow region). (Right) Experimental $i–t$ signal for cell arrival (adsorption) and retreat (collision). The linear velocity $T/\Delta t$ was used to convert i-distance points (left) into experimental $i–t$ pairs (right).

The left side of Scheme 2 shows steps to simulate current as a function of cell (red) locus until reaching the value i_B at distance T. On the right side, an experimental i–t profile depicts an adsorptive event (current step) along with a bouncing collision (blip). From experiments we can determine Δt of arrival (front of the signal) and retreat (tail of the blips). The "contactless passage" (not shown) can be thought of as a blip for which the cell does not touch the UME surface. For both types of blips, we assumed the arrival and retreat occurred in the same direction (Scheme 1).

Matching experimental i–t collision signals. We assume that any cell displacement simulated in the T-region correlates with a concomitant elapsed time Δt in the experimental signal according to the average velocity $T/\Delta t$. By "cell displacement" we mean two cell loci simulated independently, rather than real time motion of the cell (Schemes 1 and 2). To simulate the i–t values of an experimental signal (*i.e.* arrival or retreat), we first applied the sum of least squares method to select the angle with best fit. Then we proceeded to match specific i–t points on the experimental trace. We used the interpolation method,[12] whereby after simulating i_T for a desired cell locus, we calculate the time (t_T) it takes to reach that point from (or to) T at velocity $T/\Delta t$. The procedure is iterated to match the desired number of data points, but the outcome is entirely controlled by the experimental value Δt and the simulated parameter T. Following these steps, we simulated different conditions of r_c, r_e, and C_{FCN}, observing deviations in Δi ($\Delta i = i_B - i_s$ in Scheme 2) with respect to experimental values ranging from 1.4 to 5.8% (Table S1, ESI†). Such differences remain similar to previous work,[3,12] and they may be due to considering diffusion as the exclusive mode of transport for FCN while ignoring its electromigration.[12] The latter likely contributes to FCN transport resulting from the low ratio of supporting electrolyte (KCl) to FCN (<1) in Fig. 1. For migration to be negligible in redox species transport, this ratio should be >50.[27]

T-Dependence on r_c/r_e. To establish the effect of the ratio r_c/r_e on the value of T, the latter was simulated as a function of the electrode radius (6, 12.5, 15, and 22.5 μm) while keeping t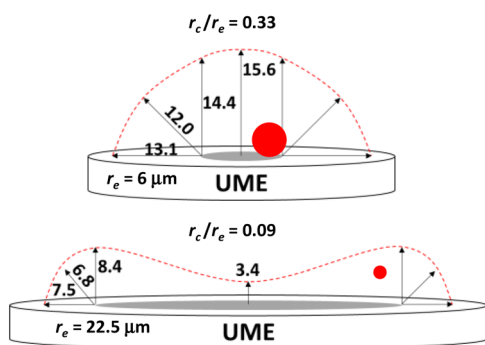he cell radius constant at 2 μm. Fig. 2, shows that when the ratio r_c/r_e is 0.33 using the smallest UME, the T-region displays a quasi-hemispherical profile with almost uniform T-values (~3 cell diameters) around the UME, including part of the shroud (Fig. 2). In contrast, for the largest electrode (r_c/r_e = 0.09), T-values decrease overall, but much more at the center (<1 cell diameter) than the edge (~2 cell diameters), thereby generating an "edge effect". This in turn reflects the mediator flux difference in disk UMEs between center (planar) and edge (radial).[26] The T-values in Fig. 2 were obtained assuming a time-independent diffusion layer because of the steady-state flux of mediator typical of UMEs.[28]

To evaluate ratios of r_c/r_e higher than 0.33 (Fig. 2), we compared values of simulated Δi at edge and center for every electrode as a function of cell radius. Each data point in Fig. 3 represents a simulation of Δi done at the edge and center of a UME with radius 6 μm, while varying cell radius. Fig. S5, (ESI†) shows identical plots for other electrode dimensions. Table 1 summarizes the cell radii for the electrode sizes in this study at which Δi-values from edge and center become equal. In all cases the ratio r_c/r_e to attain that point is about 0.7.

Based on experiments and simulations, Δi has been found to be proportional to i_B and the square of the ratio, r_c/r_e, following the empirical expression:[29]

$$\Delta i = i_B \left(\frac{r_c}{r_e}\right)^2 \tag{1}$$

which indicates that for a collision to be observable, the ratio r_c/r_e should be at least ~0.1, to induce a ~1% change on the bare UME current.[29] This prediction agrees with the i–t plot for electrode radius 22.5 μm (r_c/r_e = 0.09) in which signals are barely detectable from the noise (Fig. 1B). Eqn (1) is only approximate, as it does not consider the flux difference between center and edge. Recently, a modified version was proposed:[10]

$$\frac{\Delta i}{i_B} = F_g \left(\frac{r_c}{r_e}\right)^2 \tag{2}$$

where F_g is a geometric factor dictated by landing location on the UME.[10] Therefore, F_g takes on a different value for center and edge landings, and can be obtained by evaluating the slope of plots of $\Delta i/i_B$ *versus* $(r_c/r_e)^2$ from experiments and/or simulations.[10,20] For each electrode radius here, we determined F_g at the edge and center using simulated values of Δi
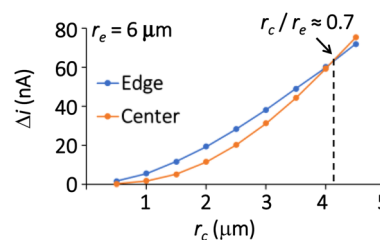

Fig. 2 Simulated T-values (μm) as the ratio r_c/r_e decreases for a cell (r_c = 2 μm, red circle and dot, not drawn to scale) hovering on the right side of the UMEs.

Fig. 3 Simulated Δi-values (center and edge) for a UME r_e = 6 μm. Dashed line shows r_c-value at which both equalize.

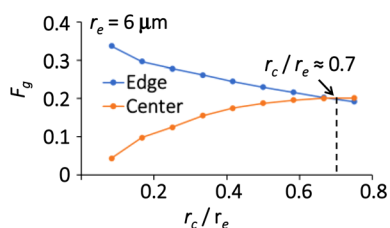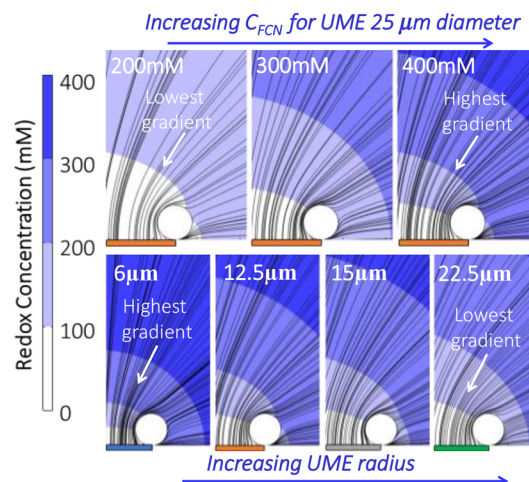**Table 1** Conditions equalizing edge-center Δi-values[a]

r_e (μm)	r_c (μm)	r_c/r_e
6	4.0	0.67
12.5	8.5	0.68
15	10	0.67
22.5	15	0.67

[a] From simulations.

and i_B, while increasing cell radius. Fig. 4 shows values of F_g for center and edge as a function of the ratio r_c/r_e. The maximum difference between the two landings locations occurs at ratio ~0.1, the value representing the limit of detection for this technique.[29] When the ratio reaches ~0.67, both center and edge F_g-values attain equal magnitude, indicating that eqn (1) could be used to calculate cell size accurately from Δi measurements. Identical plots displaying almost the same ratio were obtained for the other electrode sizes (Fig. S6, ESI†).

To understand how ~0.7 emerges as magic ratio to dissipate the "edge effect" in Δi, we show in Fig. 5 simulation snapshots of the cell located at the UME edge as it perturbs J_{FCN} while increasing C_{FCN} and electrode diameter. As indicated by the vertical bar on the top left side, a darker shade of blue represents a higher value in C_{FCN} while flux lines indicate the gradient direction towards the UME surface. Experimentally it is found that the magnitude of Δi scales up with mediator concentration.[1–3] On the other hand, eqn (1) predicts an inverse relationship between Δi and electrode size. Connecting these relationships with the shades of blue in Fig. 5, one can easily see that the higher the concentration gradient and number of gradient layers simultaneously obstructed by the sphericity of the cell, the higher Δi (see C_{FCN} = 400 mM and r_e = 6 μm). In agreement with this tendency, J_{FCN} at the UME edge, goes from ~0.19 to ~0.38 mol cm^{-2} s^{-2} when raising C_{FCN} from 200 to 400 mM (Fig. S7A, ESI†). Likewise, increasing the electrode diameter in Fig. 5, causes J_{FCN} at the edge to raise from ~0.7 to ~0.2 mol cm^{-2} s^{-2} (Fig. S7B, ESI†). Therefore, in both cases, the more flux blocked (high C_{FCN} or small r_e), the higher Δi. The effect caused by the size of the cell interfering simultaneous number of gradient layers, is also observed in simulation snapshots acquired at 90°, 45°, and 0° from the UME edge (Fig. S8, ESI†).

Due to the hemispherical profile of the flux, changing the angle at constant distance from the UME edge, keeps the cell
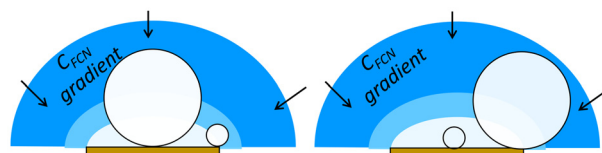

Fig. 5 Simulation snapshots of mediator flux disruption by cell with r_c = 2 μm at UME edge when increasing C_{FCN} (top) and r_e (bottom).

almost in the same concentric layer of flux. Therefore, T-values obtained at those angles are similar (Fig. 2). Because blocking signals truly arise from perturbing mediator flux, even when the cell resides at the surface, we attribute the morphing of the T-region in Fig. 2, to the way a large cell (r_c/r_e ~0.7) obstructs J_{FCN} in comparison to a small one (r_c/r_e ~0.1).

Scheme 3 pictorially depicts a hemispherical gradient of C_{FCN} with arrows representing J_{FCN} and circles outlining the two types of spherical cells at center and edge locations. A large cell offsets the flux deficit at the center by perturbing farther layers of concentration gradient, plus some part of the edge flux. In contrast, a small cell has only access to the decreased center flux, whereas at the edge, the same small cell perturbs "more" gradient layers and a heightened flux. This is a result of J_{FCN} being proportional to the concentration gradient of C_{FCN} and D_{FCN} following Fick's law.[26] It turns out, the ratio r_c/r_e ~0.7, renders a suitable perturbation profile such that the "edge effect" from nonuniform flux ends up evening out. Consequently, when reaching this ratio, eqn (1) is expected to provide accurate prediction of size from Δi without knowing cell landing location.

Signal shape

Fig. 6 shows three major types of signals (A–C) observed in i–t recordings with various electrode radii (6, 12.5, 15 and 22.5 μm) displayed as $\Delta i/i_B$. The triangle symbols come from simulated currents following the procedure in Scheme 2,

Fig. 4 Simulated F_g-values (edge and center) for r_e = 6 μm.

Scheme 3 Depiction of edge and center blocking of J_{FCN} (arrows) for spherical cells at r_c/r_e ~0.7 (large) and ~0.1 (small).
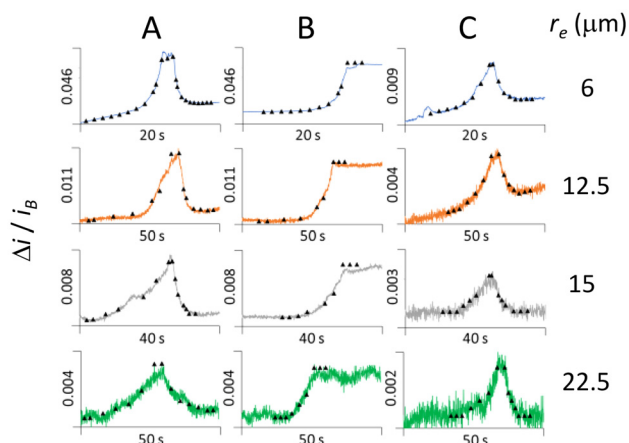
Fig. 6 Collision signals represented as $\Delta i/i_B$ (line) and matched currents (triangles) at Pt UMEs with 48 fM cells, 400 mM FCN, 100 mM KCl. +0.6 V *vs.* Ag/AgCl from i–t traces in Fig. 1. (A) Large blip (bouncing collision); (B) step (adsorption); (C) small blip (contactless passage).

wherein cells are represented as spheres of radius 2 μm arriving to the UME edge. Assuming edge landings is justified by the "electrophoretic edge effect",[14] whereby particles tend to land and accumulate at the edge as verified with electrochemical microscopy.[3,13–15] The best matches occurred for arrival angles of 90° and 45°, when using 1.22×10^{-9} cm^2 s^{-1} as cell diffusion coefficient (r_c = 2 μm) instead of 0.61×10^{-9} cm^2 s^{-1} estimated for budded cells ($r_c \approx 4$ μm). Despite the bimodal distribution of cell diameter observed with the microscope (see Experimental section), we believe sedimentation precludes any of the budded cells reaching the UME.[16]

Our assignments in Fig. 6 are consistent with recent correlated microscopy of nanodroplet blocking impacts.[17] For example, "large" blips (A) are attributed to bouncing collisions,[17] current steps (B) represent adsorption events,[1] and "small" blips, are ascribed to contactless passages.[17] Small blips display lower current than large blips and steps, and do not match simulated signal for r_c = 2 μm at the edge. It is important to emphasize that the matched currents (triangles) in Fig. 6 are obtained by assuming a linear collision velocity, which is untrue for the non-homogeneous electric field around the UME.[7,9] However, we demonstrate that our nontransport model is capable of producing average velocity values that match experimental currents assuming generic collision types. Finally, we interpret the truncated feature observed in some blips (Fig. 6A, r_e = 6 μm) as characteristic of multi-collisional encounters driven by Brownian fluctuations before the cell wanders off the UME. Such behavior has been observed in experiments and simulations of highly diffusive entities like Ag-nanoparticles[30–33] and toluene microdroplets with low ζ-potential.[34]

Cell transport

The dominant mode of cell transport is attributed to electromigration driven by the negatively charged cells (zeta potential

= −16 mV ± 4 mV) and the positive UME oxidizing FCN. When reversing the polarity of the UME (r_e = 12.5 μm) negatively to reduce ferricyanide, we did not detect collision signals (ESI, Fig. S4†). It is also likely that some electroosmosis induced by the shroud, may contribute to electromigration, as it has been documented with bacteria in similar conditions of electrolyte and redox mediator.[8,9,13] Therefore, the combined transport contribution can be expressed by:[7]

$$J = J_{\text{diff}} + J_{\text{mig}} + J_{\text{conv}} \quad (3)$$

where J represents the total flux of cells reaching the UME, while J_{diff}, J_{mig}, and J_{conv}, symbolize the contributions from diffusion, migration, (*i.e.* electromigration) and convection. Given that concentration gradients of cells induced at the UME surface by adsorptive events is rather marginal, J_{diff} should also be minor. However, random walk fluctuations in position δ, will always be present following the expression:[35]

$$\delta = \frac{2D_c}{v_a} \quad (4)$$

where D_c is the diffusion coefficient (1.22×10^{-9} cm^2 s^{-1}) for a cell of r_c = 2 μm, estimated using the Einstein–Stokes relation,[26] and v_a is the arrival velocity by migration, in this case estimated from $T/\Delta t$ (see above). The distance parameter δ represents the scope of random variations in position driven by Brownian fluctuations as the cell arrives with velocity v_a due to migration.[35] So, the time (τ) spent by the cell wandering away a distance δ while arriving at velocity, v_a, is $\tau = \delta_a/v_a$.[35] Replacing τ in the Einstein's expression for Brownian fluctuations ($\delta^2 = 2D\tau$) gives eqn (4).[35,36]

Table 2 lists T-values along with dynamic parameters estimated for collision events in i–t plots from Fig. 6 as a function of r_e. The magnitude of T constitutes the farthest distance from the UME at which perturbations of J_{FCN} become detectable on the baseline current response. As the electrode radius shrinks, T-values grow with a steep rise for the smallest electrode when the ratio r_c/r_e increases enough to mitigate the influence of the edge effect (Fig. 2). To calculate v_a we only used the Δt-value corresponding to the tail of the selected signal (Scheme 2). The arrival cell velocities (Table 2) for all UMEs are similar, except for the smallest one that appears slightly higher (1.6 *versus* ~0.7 μm s^{-1}). Therefore, Brownian fluctuations (δ = 0.15–0.4 μm) are more likely to offset migration trajectories on the large UMEs than the smallest one, because those fluctuations are of comparable magnitude

Table 2 Dynamic parameters from collision signals at different UME radius

r_e (μm)	**6**	**12**	**15**	**22.5**
T^a (μm)	14.4	9.8	8.9	8.4
n^b	5	32	25	70
v_a (μm s^{-1})	1.6 ± 0.5	0.7 ± 0.2	0.6 ± 0.3	0.6 ± 0.3
δ (μm)	0.15 ± 0.05	0.3 ± 0.1	0.4 ± 0.2	0.4 ± 0.2
v_r (μm s^{-1})	2.2 ± 0.7	1.3 ± 0.5	1.1 ± 0.3	0.8 ± 0.3

^{a} Determined at UME edge 90° angle. ^{b} Number of events analyzed.

with the average arrival velocity (0.7 to 0.6 µm s^{-1}) on large UMEs. The electric field also gets "diluted" on an increased electrode area. Correspondingly, the smallest electrode, r_e = 6 µm, displays a heightened value of v_a with low degree of Brownian fluctuations (δ).

Retreat velocities (v_r) were also estimated using the Δt-value from the front of the blip signal (Scheme 2). They appear slightly higher in magnitude than v_a because of using the same T-values (direction) of arrival in the ratio $T/\Delta t$. It is unlikely that a cell leaves the T-region in the same direction it arrived. Therefore, the somewhat increased values of v_r suggests boosted retreat speeds by shroud-induced electroosmotic flow,[8,9,13] and/or sedimentation.[16] Also, when comparing slopes of tail and front for blips in Fig. 6, one can guess which trip (arrival or retreat) appears faster. In some cases, the blip slopes are similar and in others the retreat appears faster. The velocities (arrival and retreat) shown in Table 2 are comparable to values determined for *E. coli* and *B. subtilis*, 0.7 to 4.5 µm s^{-1},[12] respectively, as well as for *L. lactis*,[8] whose velocity has been measured in the vicinity of UMEs under different conditions of electroosmotic flow (~5 to 50 µm s^{-1}).[8] We can also compare with sedimentation rates recently determined in electrochemical blocking of yeast cells under electrolyte conditions similar to ours.[16] The researchers estimated settlement rates of ~0.26 µm s^{-1}, which ranges ~20 to 40% of the values for speed arrival observed with the UMEs in Table 2. As expected, the smallest UME experiences the least sedimentation effect due to its strongest electric field.

Conclusions

We have investigated single collisions of yeast cells using disk Pt-UMEs of varying diameter. A combination of experiments and simulations led us to several new findings. First, we estimated average collision velocities that comply with underlying theory of particle transport in electrochemical cells and values reported in other studies. We can use these average velocities to match current–time profiles in experimental impact signals for three generic collisions (adsorption, bouncing collision, and contactless passage). Second, we determined a theoretical value of ~0.7 for the ratio r_c/r_e at which the "UME-edge effect", is expected to cease impairing accuracy of size estimates. Though we did not test this prediction, it makes intuitive sense because once the diameter of particle and electrode becomes close, the difference of redox flux between edge and center at the UME should stop affecting the blocking profile. Third, cells electromigrate towards UMEs arriving at average velocities that are counteracted by random walk fluctuations and sedimentation. Both effects decrease when using smaller UMEs that harbor stronger electric fields. Electroosmotic flow driven by the shroud surface may also play a role for the apparent increased retreat velocities observed in blip signals attributed to bouncing collisions and contactless passages. Finally, our model predicts a sensitive region around the UME, (including the shroud) demarcated by a threshold distance T

wherein cells encode their dynamics by perturbing mediator flux. Outside this region, cell motion becomes undetectable because any flux disruption falls within the noise level established by the ratio r_c/r_e and mediator flux. The T-region represents the sensitivity of electrochemical blocking experiments and can be improved by increasing the ratio r_c/r_e or mediator concentration. Though T-values have been determined in past simulations,[2,3] the role of T in delineating a finite region of sensitivity around the UME that serves to encode particle dynamics has never been demonstrated explicitly, likely because the signals available at the time had "zero" duration.[2,3] Our findings represent a step forward in the quest to better understand the challenges of stochastic blocking electrochemistry and ways to mitigate them.

Author contributions

J. A. Lutkenhaus and J. U. Ahmed conceived and designed experiments and simulations; J. A. Lutkenhaus conducted experiments, curated data, prepared figures, and wrote experimental section and ESI.† M. Hasan and J. U. Ahmed prepared Simulation report. D. C. Prosser, cultured cells and provided expertise on yeast. J. C. Alvarez wrote manuscript drafts and curated data. All authors reviewed the manuscript.

Conflicts of interest

There are no conflicts to declare.

Acknowledgements

References

1 B. M. Quinn, P. G. van't Hof and S. G. Lemay, Time-Resolved Electrochemical Detection of Discrete Adsorption Events, *J. Am. Chem. Soc.*, 2004, **126**, 8360–8361.

2 A. Boika, S. N. Thorgaard and A. J. Bard, Monitoring the Electrophoretic Migration and Adsorption of Single Insulating Nanoparticles at Ultramicroelectrodes, *J. Phys. Chem. B*, 2013, **117**, 4371–4380.

3 S. E. Fodsdick, M. J. Anderson, E. G. Nettleton and R. M. Crooks, Correlated Electrochemical and Optical Tracking of Discrete Collision Events, *J. Am. Chem. Soc.*, 2013, **135**, 5994–5997.

4 L. A. Baker, Perspective and Prospectus on Single-Entity Electrochemistry, *J. Am. Chem. Soc.*, 2018, **140**, 15549–15559.

5 Z. Deng and C. Renault, Detection of Individual Insulating Entities by Electrochemical Blocking, *Curr. Opin. Electrochem.*, 2021, **25**, 100619.

6 J.-H. Park, A. Boika, H. S. Park, H. C. Lee and A. J. Bard, Single Collision Events of Coductive Nanoparticles Driven by Migration, *J. Phys. Chem. C*, 2013, **117**, 6651–6657.

7 S. G. Lemay, C. Renault and J. E. Dick, Particle Mass Transport in Impact Electrochemistry, *Curr. Opin. Electrochem.*, 2023, **39**, 101265.

8 S. N. Thorgaard, S. Jenkins and A. R. Tarach, Influence of Electroosmotic Flow on Stochastic Collisions at Ultramicroelectrodes, *Anal. Chem.*, 2020, **92**, 12663–12669.

9 T. Moazzenzade, X. Yang, L. Walterbos, J. Huskens, C. Renault and S. G. Lemay, Self-Induced Convection at Microelectrodes via Electroosmosis and its Influence on Impact Electrochemistry, *J. Am. Chem. Soc.*, 2020, **142**, 17908–17912.

10 J. Bonezzi and A. Boika, Deciphering the Magnitude of Current Steps in Electrochemical Blocking Collision Experiments and Its Implications, *Electrochim. Acta*, 2017, **236**, 252–259.

11 J. H. Chung, J. L. Jiseon, J. Hwang, K. H. Seol, K. M. Kim, J. Song and J. Chang, Stochastic Particle Approach Electrochemistry (SPAE): Estimating Size, Drift Velocity, and Electric Force of Insulating Particles, *Anal. Chem.*, 2020, **92**, 12226–12234.

12 J. U. Ahmed, J. A. Lutkenhaus, A. Tubbs, A. Nag, J. Christhopher and J. C. Alvarez, Estimating Particle Arrival Velocities Using th Time Variation of the Current Signal in Stochastic Blocking Electrochemistry, *Anal. Chem.*, 2022, **94**, 16560–16569.

13 A. T. Ronspees and S. N. Thorgaard, Blocking Electrochemical Collisions of Single *E. coli* and B. subtilis bacteria at Ultramicroelectrodes Elucidated Using Simultaneous Fluorescence Microscopy, *Electrochim. Acta*, 2018, **278**, 412–420.

14 T. Moazzenzade, T. Walstra, X. Yang, J. Huskens and S. G. Lemay, Ring Ultramicroelectrodes for Current-Blockade Particle-Impact, *Anal. Chem.*, 2022, **94**, 10168–10174.

15 A. D. Pendergast, C. Renault and J. E. Dick, Correlated Optical -Electrochemical Measurements Reveal Bidirectional Current Steps for Graphene Nanoplatelet Collisions at Ultramicroelectrodes, *Anal. Chem.*, 2021, **93**, 2898–2906.

16 H. Zhang, G. Gao, Y. Chen, L. Lin, D. Wang, Y. Fan, Y. Liu, Q. Zhao and J. Zhi, Effect of Cell Settlement on the Electrochemical Collision Behaviors of Single Microbes, *Anal. Chim. Acta*, 2023, **1283**, 341949.

17 K. J. Vannoy, C. Renault and J. E. Dick, The Microelectrode Insulator Influences Water Nanodroplet Collisions, *Anal. Chem.*, 2023, **95**, 7286–7293.

18 E. Suraniti, F. Kanoufi, C. Gosse, X. Zhao, R. Dimova, B. Pouligny and N. Sojic, Electrochemical Detection of Single Microbeads Manipulated by Optical Tweezers in the Vicinity of Ultramicroelectrodes, *Anal. Chem.*, 2013, **85**, 8902–8909.

19 Z. Deng, R. Ellatar, F. Maroun and C. Renault, In Situ Measurement of the Size Distribution and Concentration of Insulating Particles by Electrochemical Collision on Hemispherical Ultramicroelectrodes, *Anal. Chem.*, 2018, **90**, 12923–12929.

20 J. Chung, P. Hertler, K. W. Plaxco and L. Sepunaru, Catalytic Interruption Mitigates Edge Effects in the Characterization of Heterogeneous, Insulating Nanoparticles, *J. Am. Chem. Soc.*, 2021, **143**, 18888–18898.

21 J. Y. Lee, B. K. Kim, M. Kang and J.-H. Park, Label-Free Detection of Single Living Bacteria via Electrochemical Collision Event, *Sci. Rep.*, 2016, **6**, 30022.

22 G. Gao, D. Wang, R. Brocenschi, J. Zhi and M. V. Mirkin, Toward the Detection and Identification of Single Bacteria by Electrochemical Collision Technique, *Anal. Chem.*, 2018, **90**, 12123–12130.

23 T. L. T. Ho, N. T. T. Hoang, J. Y. Lee, H. J. Park and B. K. Kim, Determining Mean Corpuscular Volume and Red Blood Cell Count Using Electrochemical Collision Events, *Biosens. Bioelectron.*, 2018, **110**, 155–159.

24 L. Danis, D. Polcari, A. Kwan, S. M. Gateman and J. Mauzeroll, Fabrication of Carbon, Gold, Platinum, Silver, and Mercury Ultramicroelectrodes with Controlled Geometry, *Anal. Chem.*, 2015, **87**, 2565–2569.

25 S. J. Konopka and B. McDuffie, Diffusion Coefficients of Ferri- and Ferrocyanide Ions in Aqueous Media, Using Twin-Electrode Thin-Layer Electrochemsitry, *Anal. Chem.*, 1970, **42**, 1741–1746.

26 A. J. Bard, L. R. Faulkner and H. S. White, *Electrochemical Methods: Fundamentals and Applications*, Wiley, New York, 3rd edn, 2022.

27 H. Zhao, J. Chang, A. Boika and A. J. Bard, Electrochemistry of High Concentration Copper Chloride Complexes, *Anal. Chem.*, 2013, **85**, 7696–7703.

28 J. Heinze, Ultramicroelectrodes in Electrochemistry, *Angew. Chem., Int. Ed. Engl.*, 1993, **32**, 1268–1288.

29 J. E. Dick, C. Renault and A. J. Bard, Observation of Single-Protein and DNA Macromolecule Collisions on Ultramicroelectrodes, *J. Am. Chem. Soc.*, 2015, **137**, 8376–8379.

30 D. A. Robinson, Y. Liu, M. A. Edwards, N. J. Vitti, S. M. Oja, B. Zhang and H. S. White, Collision Dynamics during the Electrooxidation of Individual Silver Nanoparticles, *J. Am. Chem. Soc.*, 2017, **139**, 16923–16931.

31 W. Ma, H. Ma, J.-F. Chen, Y.-Y. Peng, Z.-Y. Ynag, H.-F. Wang, Y.-L. Ying, H. Tian and Y.-T. Long, Tracking Motion Trajectories of Individual Nanoparticles Using Time-Resolved Current Traces, *Chem. Sci.*, 2017, **8**, 1854–1861.

32 J. Ustarroz, M. Kang, E. Bullions and P. R. Unwin, Impact and Oxidation of Single Silver Nanoparticles at Electrode

Surfaces: One Shot Versus Multiple Events, *Chem. Sci.*, 2017, **8**, 1841–1853.

33 S. M. Oja, D. A. Robinson, N. J. E. Vitti, M. A. Edwards, Y. Liu, H. S. White and B. Zhang, Observation of Multipeak Collision Behavior during the Electrochemical Oxidation of Single Ag Nanoparticles, *J. Am. Chem. Soc.*, 2017, **139**, 708–718.

34 J. U. Ahmed, J. A. Lutkenhaus, M. S. Alam, I. Marshall, D. K. Paul and J. C. Alvarez, Dynamics of Collisions and Adsorption in the Electrochemistry of Individual Emulsion Microdroplets, *Anal. Chem.*, 2021, **93**, 7993–8001.

35 H. C. Berg, *Random Walks in Biology*, Princeton University Press, Princeton, New Jersey, 1993.

36 A. Einstein, Uber die von der molekularkinetischen Theorie der Warme geforderte Bewegung von in ruhenden Flussigkeiten suspendierten Teilchen, *Ann. Phys.*, 1905, **322**, 549–560.